VIP *Very Important Paper*

Coacervate-Droplet Cased Synthetic Cells Regulated By Activated Carboxylic Acids (ACAs)

Matteo Valentini,[a] Stefano Di Stefano,*[a] and Job Boekhoven*[b]

Regulating the formation and dissolution of active complex coacervate droplets with chemical reactions offers a powerful synthetic cell model. Such active droplets are also helpful in understanding the non-equilibrium nature of membrane-less organelles. Like many membrane-less organelles, these droplets rely on high-chemical potential reagents, like ATP, to maintain their transient nature. This study explores Activated Carboxylic Acids (ACAs) as a high-chemical potential fuel to modulate the lifetime of peptide-based coacervates through transient pH changes. We demonstrate that nitroacetic acid, a commonly used ACA, can effectively induce the formation and dissolution of coacervates by transiently altering the solution's pH. The

system, comprising the zwitterionic peptide Ac-FRGRGD-OH and polyanions, forms coacervates upon protonation at low pH and dissolves as the pH returns to neutral. Our findings indicate that the lifetime of these synthetic cells can be fine-tuned by varying the amount of ACA added, and the system can be refueled multiple times without significant interference from by-products. This ACA-driven reaction cycle is versatile, accommodating various coacervate compositions and enabling the uptake of diverse compounds, making it a valuable model for compartmentalization. The study underscores the potential of ACA-fueled coacervates as a platform for investigating biomolecular condensates and developing synthetic life systems.

Introduction

Membrane-less organelles, or biomolecular condensates, are formed through liquid-liquid phase separation via many weak interactions between macromolecules like proteins and RNA interactions.[1–3] Examples include the formation of the centrosomes and Cajal bodies, which are critically important in regulating cellular functions. These droplets find themselves in the active, non-equilibrium environment of the cell. Moreover, the formation of these droplets is frequently coupled to non-equilibrium reaction cycles such as transient phosphorylation, methylation, and acetylation.[5–8] For example, phosphorylation and dephosphorylation of a protein regulate the phase separation of neuronal granules that, in turn, regulate mRNA translation.[9,10] Such transient phosphorylation of a protein by consuming fuels like ATP can induce a precursor's reversible, transient transformation into a building block able to bind

other components like RNA to form complex coacervates. The active droplets emerge and persist only briefly due to their low stability. They can emerge, persist, or decay depending on the availability of fuel. The latter regulates when and where organelles assemble and disassemble and their shape, size, and functions. All these exciting properties (*i.e.*, emergence, persistence, decay, collective behavior, and self-division) are pivotal to the functioning of life.

There is a growing interest in active materials,[11–21] such as active droplets.[22–24] Coacervation is sometimes coupled to dissipative cycles involving enzymatic reactions[25,26], which require complex components and narrow conditions. In other cases, simpler reaction cycles were designed, which resort to smaller molecules to induce the transient formation of coacervates in a more prebiotically plausible fashion. Carbodiimides are exploited as chemical fuels (here, the term "fuel" is used for chemical species that drive the formation of active droplets in an out-of-equilibrium state).[27–31] Active droplets can be obtained in water employing a zwitterionic peptide as a precursor, which, in the presence of the carbodiimide, is activated to a cationic form featured by an increased affinity for a polyanion. When enough peptide is activated, it phase-separates, forming droplets. The complex coacervate-based droplets form spontaneously and decay without additional fuel. Recently, a new reaction cycle has been reported, which uses a monoamidophospate that transiently phosphorylates a histidine–containing peptide. The latter undergoes phase separation in the presence of different polyanions. The hydrolysis of the peptide leads to the dissolution of the coacervates.[32] A common drawback of both reaction cycles is their sensitivity to the presence of other compounds (*i.e.*, electrophiles and nucleophiles) that can interfere, leading to detrimental side reactions. Moreover, in the case of the carbodiimide fuel, the urea-derivative waste product, being a denaturing agent, is usually

[a] *Department of Chemistry, Università di Roma La Sapienza and ISB-CNR Sede Secondaria di Roma – Meccanismi di Reazione, Roma, Italy*
[b] *Department of Bioscience, School of Natural Sciences, Technical University of Munich, Garching, Germany*

Correspondence: *Stefano Di Stefano, Department of Chemistry, Università di Roma La Sapienza and ISB-CNR Sede Secondaria di Roma – Meccanismi di Reazione, P.le A. Moro 5, I-00185 Roma, Italy.*
Email: stefano.distefano@uniroma1.it

Job Boekhoven, Department of Bioscience, School of Natural Sciences, Technical University of Munich, Lichtenbergstrasse 4, 85748 Garching, Germany.
Email: job.boekhoven@tum.de

ChemSystemsChem

Research Article
doi.org/10.1002/syst.202400083

**Chemistry
Europe**
European Chemical
Societies Publishing

problematic for refueling experiments or for other structurally complex components like enzymes.

In nature, liquid-liquid phase separation to form membrane-less organelles can also be obtained through cytoplasmic pH variations in response to cellular stress.[33,34] This approach has been widely used to control the behavior of active materials, and in particular, it has been shown that activated carboxylic acids (ACAs)[35] can drive chemical reaction cycles by temporarily changing the pH of the solution in a dissipative fashion.[36–38] Upon addition of the ACA, the solution goes through a fast pH drop, and the components in the system pass from a neutral resting state A to a protonated state B. Decarboxylation of the unstable conjugate base of the ACA, and the consequent back proton transfer restore both the initial pH and the resting state of the system (state A). Remarkably, the duration of the protonated state can be modulated by varying the nature and amount of the added ACA.[39–48]

In this work, we show that the ACA reaction cycle can change the solution pH transiently and, consequently, control the emergence, persistence, and decay of peptide-based coacervates over time. Moreover, we demonstrate the compat-ibility of this reaction cycle with different coacervate composi-tions and with other compounds, showing that it is a convenient, versatile, and simple reaction cycle to study active droplet evolution as a protocell model. To achieve this aim, nitroacetic acid–an ACA commonly used in water–reaction cycle was coupled with the protonation and deprotonation of Ac-FRGRGD-OH (**1**) to transiently control the emergence and decay of peptide-based coacervates over time. Initially, at neutral pH, the system is found in an equilibrium state where the zwitterionic peptide, with a net charge equal to 0, weakly interacts with a benchmark polyanion present in the solution. When nitroacetic acid (**ACA**) is added, the pH drops to acidic values, and **1** gets protonated (**1·2H+**). Under these conditions, the peptide has a net charge of $+2$, which allows it to strongly interact with the polyanion and phase-separate into a dense coacervate phase. As the decarboxylation and back proton transfer occur, the pH rises to its initial value, and the peptide starts to deprotonate again, losing affinity for the polyanion. Consequently, the coacervate dissolves, returning the system to its initial equilibrium state (Scheme 1).
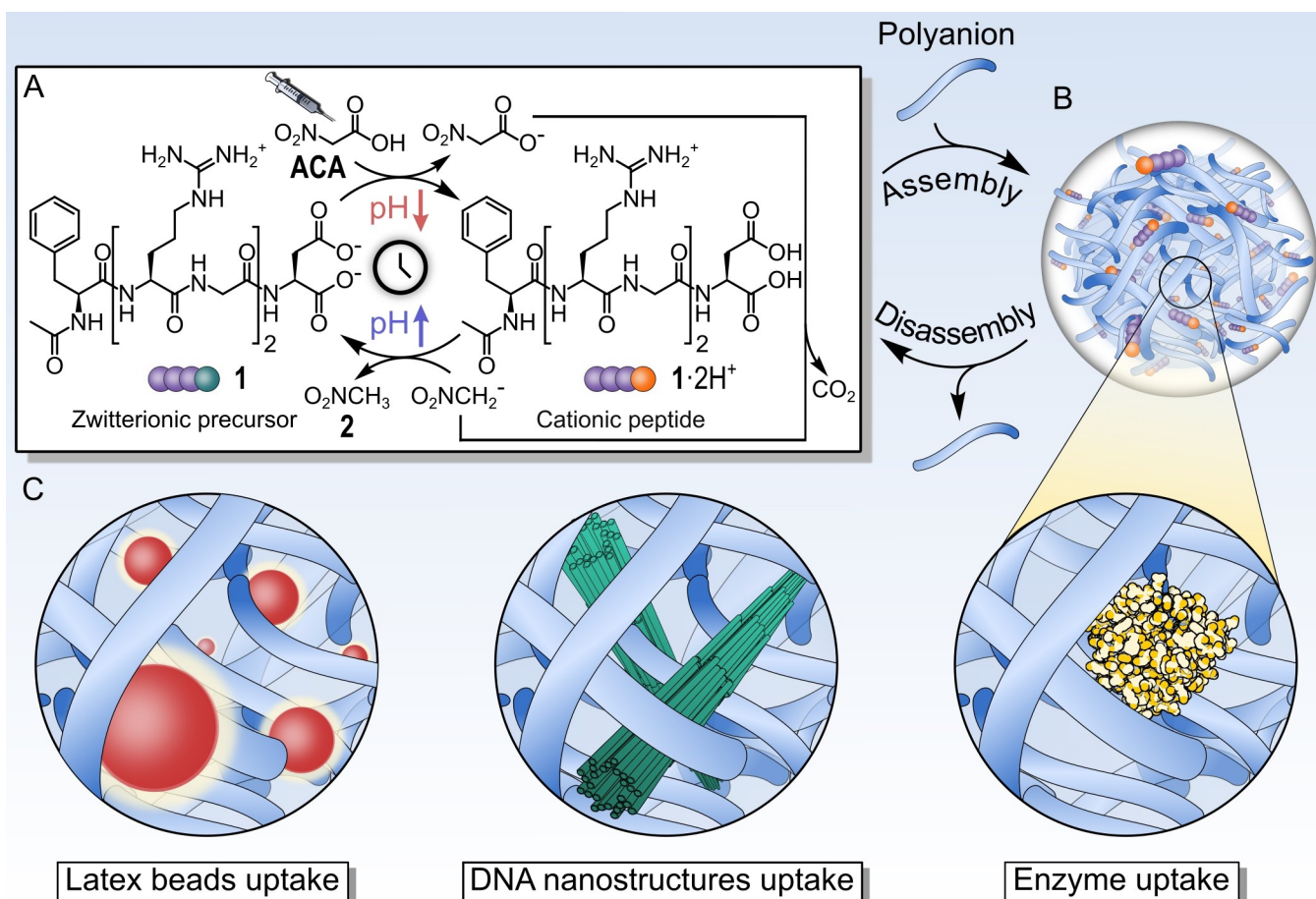
Scheme 1. Schematic representation of the nitroacetic acid (**ACA**) reaction cycle coupled to Ac-F(RG)₂D-OH (**1**) protonation and deprotonation to induce coacervation through a transient pH variation. A) Upon addition of ACA to a neutral solution of **1**, the pH drops, resulting in a transient cationic peptide (**1•2H** +) that can bind an anionic polymer (blue strand) and phase–separate into a coacervate-based droplet (B). Decarboxylation and back proton transfer of the conjugate base of **ACA** raise the pH, bringing the system back to its initial equilibrium state. C) These transient coacervates can ideally be used to uptake a wide range of compounds, such as latex beads, DNA nanostructures, and enzymes, for further applications.

ChemSystemsChem

Research Article
doi.org/10.1002/syst.202400083

**Chemistry
Europe**

European Chemical
Societies Publishing

Results and Discussion

First, different ratios of **1** to pSS₁₇ (poly(styrene sulfonate), 17 kg mol⁻¹) were screened at the plate reader. We fixed the pH at 2 in the presence of 50 mM NaCl and the plate reader measures the solution's turbidity at 600 nm as a measure of droplet formation. A well-defined phase diagram at pH 2 was obtained, showing the formation of droplets in acidic conditions (Figure S1). The specific **1** to pSS₁₇ ratio 1.25 (10 mM **1**, 8 mM pSS₁₇ (expressed in monomer concentration), 50 mM NaCl at neutral pH) was then chosen in the middle of the phase diagram to monitor the turbidity as a function of pH. The pH was varied by adding small amounts of NaOH or HCl (Figure S2). This data shows droplet formation starts when a pH value of 3.6 or lower is reached. An experiment was then performed under the same conditions, but 30 mM **ACA** was used to change the

pH transiently. The solution, initially at pH 7 and thus transparent, got turbid upon adding **ACA** due to the protonation of **1** and the formation of coacervates (Figure 1A). However, as the decarboxylation and back proton transfer occur, the pH rises to a high value, causing the slow dissolution of the coacervate phase and, eventually, restoring the initial clear solution (see Figure S3 for pH traces over time). Turbidity at 600 nm was measured over time in different fueling conditions (Figure 1B). We found that the droplet's lifetime could be tuned by changing the amount of **ACA** added to the solution (Figure 1C). The more fuel added, the longer the life cycle of the droplets. Notably, subsequent multiple fueling experiments could be performed without losing the system's efficiency, demonstrating that nitromethane (**2**), the waste product of this reaction cycle, did not significantly interfere with the droplet's lifetime cycle (Figure 1D).
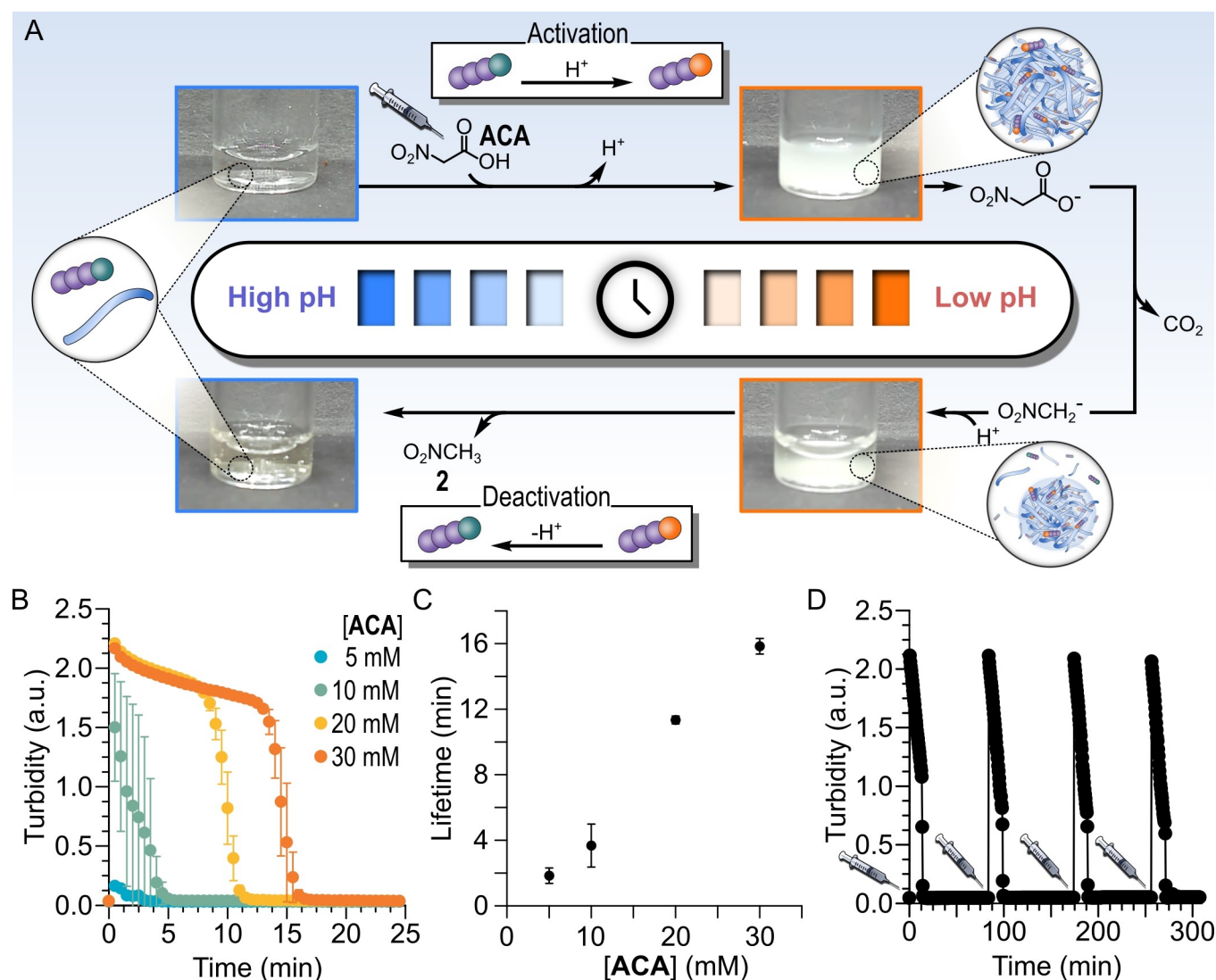

Figure 1. A) The change of solution turbidity over time upon adding 30 mM ACA to 10 mM 1, 8 mM pSS, 50 mM NaCl at pH = 7.0. B). The evolution of turbidity at 600 nm of a 10 mM 1, 8 mM pSS (50 mM NaCl, neutral pH) solution when 5 mM (light blue trace), 10 mM (light green trace), 20 mM (yellow trace), 30 mM (orange trace) of ACA are added (see also Figure S4–7) and (C) related lifetimes defined as the time needed for the turbidity to reach a value below 0.1 (a.u.) (N = 3). D) The evolution of turbidity by subsequent shots of 30 mM ACA. After each cycle, the pH was autonomously allowed to reach a value above 6.0. The lifetime of each refueling experiment is shown in Figure S8 (N = 2). The black line is a guideline for the eyes.

Microscopy experiments were carried out under the same conditions to bring visual evidence of the properties of the active droplets, *i.e.*, their emergence, decay, and collective behavior. When 30 mM of **ACA** was used, many droplets appeared due to the initial pH drop (Figure 2A). As the decarboxylation and back proton transfer proceed, the pH returns to the initial value. Throughout this time, droplets can grow through fusion (Figure 2B). Eventually, when the pH reaches a value of around 4.5, the droplets start to dissolve, passing through an out-of-equilibrium hollow shape (Figure 2D). The relatively high viscosity of these droplets (as shown by FRAP experiments in Figure 2C) compared to the ones induced by other reaction cycles[28,30,32] and the relatively fast pH increase due to the decarboxylation and back proton transfer reactions could explain why hollow coacervates are formed throughout the reaction cycle. As the pH increases, **1** gets deprotonated, and droplets tend to dissolve. However, the dissolution process, whose rate is correlated to the droplet viscosity, might be relatively slow, and it could prevent the droplets from being dissolved as quickly as the pH increases. Therefore, the droplets find themselves in a non-equilibrium state, and to overcome their instability, they assume the above hollow, transient shape. Indeed, we confirmed the slow dissolution process as the droplets in the reaction cycle are still in solution at a pH where they could not exist in in-equilibrium experiments. (see Figure S9 for further details). The appearance time of the hollow coacervates can eventually be controlled over time by using different amounts of **ACA** (Figure S10–11).

Eventually, to demonstrate that the **ACA** reaction cycle coupled to peptide-based coacervates can be used as an easy tool to study active coacervates, different polyanions with varying lengths and monomer designs, and the uptake of a wide range of chemical compounds like modified latex beads, DNA nanotubes, and enzymes were investigated. To show the wide applicability of this reaction cycle, we explored different polyanions to generate transient peptide–based coacervates. We employed the above-optimized conditions, varying the polymer design and length. When varying the polyanion length, we found the droplet lifetime increased with the polymer length (Figure 3B).[28] Noteworthy, we maintained a constant concentration of negative charges, *i.e.*, the monomer concentration remained constant. Then, different polyanions designs were investigated, including some pH-responsive polymers like poly(styrene sulfonate-co-maleate), poly(styrene-alt-maleate), (poly(acrylic-co-maleic acid)), and polyacrylate. In many of the explored kinetics, *i.e.*, dextran sulfate, polyuridylic acid, poly-(styrene sulfonate-co-maleate), the turbidity measurements and confocal microscopy suggested that droplets emerge upon the addition of 30 mM **ACA** to subsequently dissolve (Figure 3B and S16).[49] With other polyanions, *i.e.*, poly(anetholesulfonate), poly-(styrene-alt-maleate), the solution got turbid after the addition of **ACA**, but confocal microscopy showed the formation of aggregates instead of droplets, probably due to the non-optimized conditions for these polymers (Figure S16). When polyacrylate, or its derivative combined with polymaleate acid, was employed, no emergence of coacervate was observed, probably due to the high protonation of the acrylate monomer
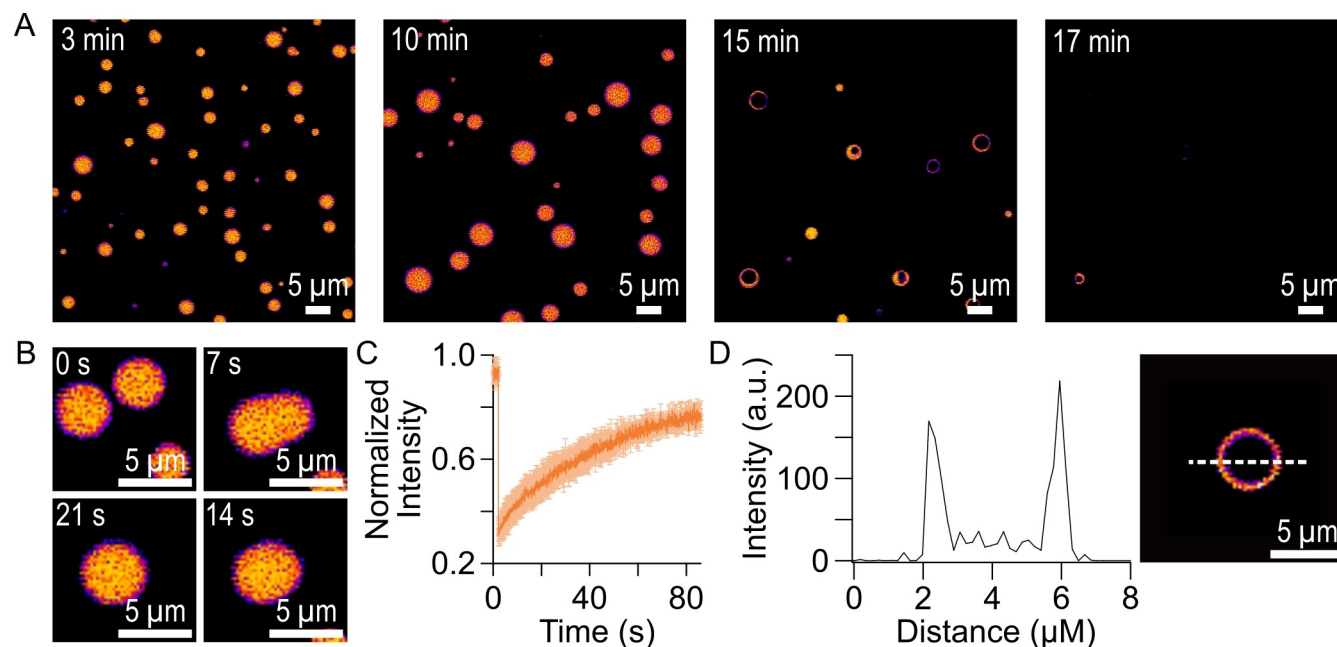

Figure 2. A) Confocal microscopy images of a 10 mM **1**, 8 mM pSS, 50 mM NaCl, and 0.1 μM sulforhodamine B solution at neutral pH after adding 30 mM **ACA**. The emergence of droplets can be observed upon fuel addition, and subsequent fusion events lead to the formation of bigger droplets. As the pH rises back to its initial value, droplets start to dissolve, and hollow coacervates can be observed as a transient morphology before the complete dissolution of the droplets. B) Confocal microscopy images showing a fusion event between two droplets. C) FRAP experiment with the fluorescently labeled peptide NBD-G(RG)^{2}D-OH shows a slow recovery with a diffusion coefficient of 0.06 μm2 s¬1 (N = 3, see Figure S12–14 for each FRAP experiment). D) A hollow droplet line profile was obtained by measuring the fluorescence along the dotted line. All experiments were performed in triplicate (N = 3), and all images' scale bars represent 5 μm.
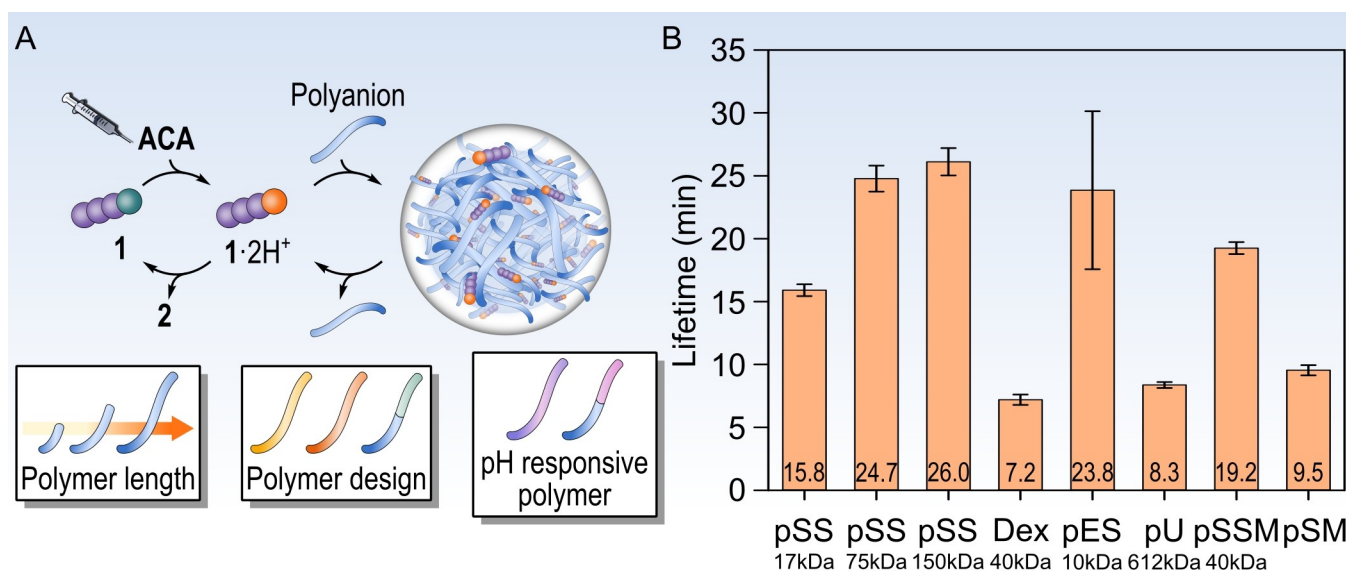
ChemSystemsChem

Research Article
doi.org/10.1002/syst.202400083

**Chemistry
Europe**
European Chemical
Societies Publishing

Figure 3. A) The effect of different polyanion lengths and designs on droplet lifetimes. B) The droplet lifetimes in an 8 mM polyanion (expressed as charge concentration), 10 mM **1**, 50 mM NaCl solution at neutral pH after addition of 30 mM ACA. Different lengths of pSS (17 kg•mol^{-1}, 75 kg•mol^{-1}, 150 kg•mol^{-1}) were used as well as different monomer structures as Dex (dextran sulfate), pES (poly(anetholesulfonate)), pU (polyuridylic acid), pSSM (poly(styrenesulfonate-co-maleate)), pSM (poly(styrene-alt-maleate)). Each polyanion's mean lifetime value is shown (N = 3). For further details and related turbidity (at 600 nm), variations over time and related confocal images, see Figure S15–16.

that causes a net decrease in the negative charge concentration (see Figure S15–16).

Active droplets have been proposed as a powerful platform for synthetic life or a model for membrane-less organelles. In these systems, the droplet functionality originates from the ability to partition reagents. We thus tested whether other components could partition into these droplets. Besides, the ability to control the partitioning in a microcompartment of different environmentally available components has always been of primary importance in explaining the emergence of functional complexity that has brought about the origin of life.[50–53] We performed a series of experiments in which the emergence and decay of droplets in the optimized conditions were coupled with the uptake of different components such as latex beads, DNA nanostructures, and enzymes (Figure 4). Amine-modified and carboxylate-modified polystyrene latex beads were partitioned inside the droplets and released after their dissolution (Figure 4 A and B, see also Figure S17–18). Remarkably, in the case of DNA nanotubes, some tubes could be observed inside the droplets immediately after adding 30 mM **ACA** (Figure 4 C). Furthermore, the DNA material was found to be organized in a spherical shell around the droplets, and it persisted even when the fuel was completely exhausted (Figure S19).

Analogously, in the case of the two enzymes, Cy5-Glucose Oxidase and Cy5-Urease were observed to be taken up by the transient droplets (Figure 4D and E, see also Figure S20–21) and eventually released after their dissolution, giving aggregates that partially retain the enzymatic activity (Figure S22). In all cases, the time interval for the dissolution of the droplets is brief and cannot be tuned by varying the concentration of ACA. We attempted to refuel the system by adding the second shot

of ACA. The droplets re-emerged and uptake both the free enzyme and the enzymatic aggregates, which stick to the boundaries of the droplets and facilitate their fusion process (Figure S23). The subsequent rise of pH dissolves the droplets and brings the formation of the solid aggregates again. The data shows that droplets can be reformed after fueling. They do show different behavior which we ascribe to the enzyme aggregate formation after the first shot.

Conclusions

We showed that activated carboxylic acid, like nitroacetic acid, can regulate the emergence and decay of peptide-based coacervates, representing a valuable approach for further investigation as synthetic cells. Our study demonstrates that an ACA-driven reaction cycle can precisely control the lifetime of the synthetic cells phase, providing a robust platform for examining early protocell-like systems. The new reaction cycles produce waste products that do not interfere with the synthetic cells. We also show that the synthetic cells readily take up functional molecules from their environment. In future works, we will functionalize these fuel-dependent, non-equilibrium synthetic cells with active molecules, like self-replicating RNA, which will be a critical step toward synthetic life.
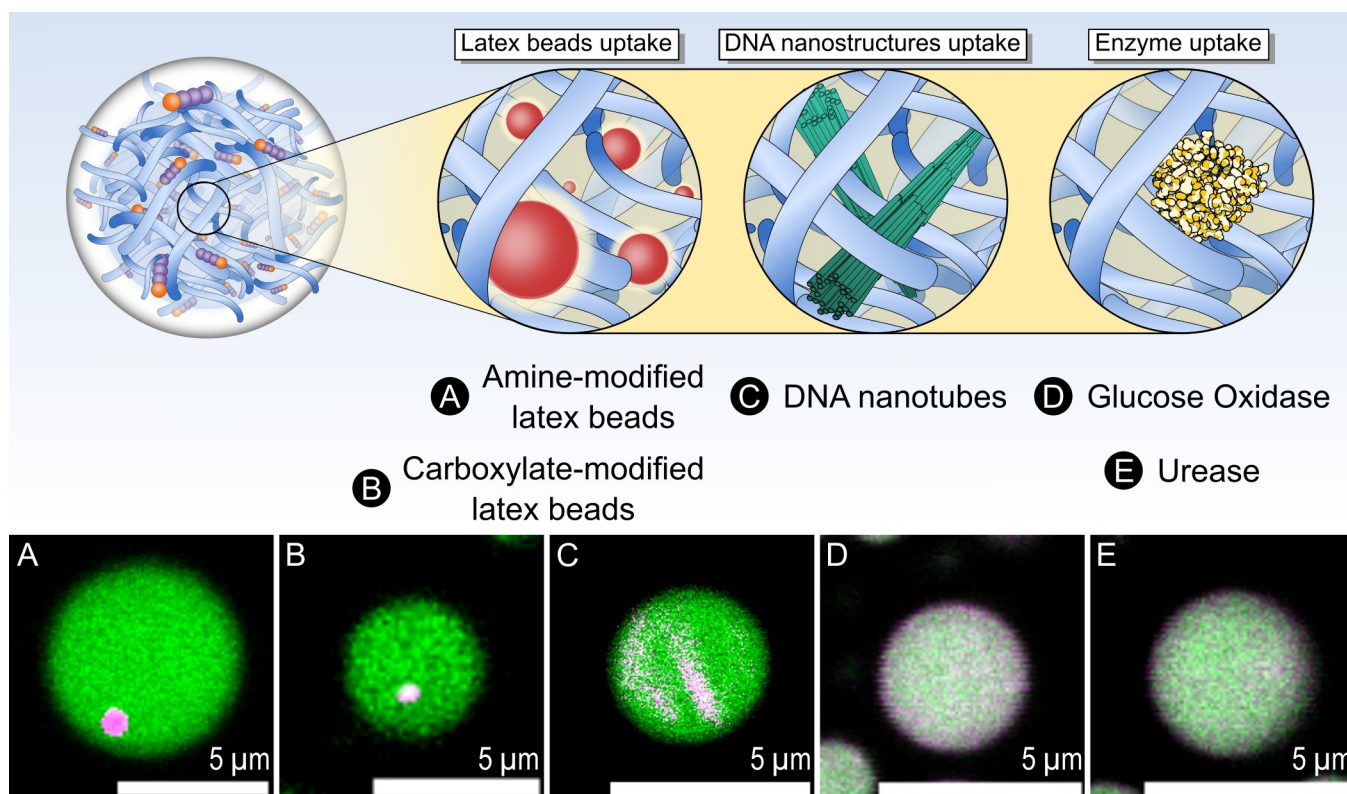
Acknowledgments

Figure 4. ACA–fueled droplets as compartments up-concentrate a wide range of chemical species during the reaction cycle. In particular, confocal microscopy images (target compound channel (magenta), droplet channel (green)) of a droplet in a 10 mM **1**, 8 mM pSS, 50 mM NaCl and amine-modified polystyrene latex beads (A) (magenta: Fluorescence Yellow-Green; green: Sulforhodamine B), carboxylate-modified polystyrene latex beads (B) (magenta: Fluorescence Red; green: NBD—G(RG)2D-OH), DNA nanotubes (100 nM of each strand 5bSE1, 5bSE2, 5bSE3, 5bSE4, 5bSE5, 5 mM MgCl2) (C) (magenta: 5bSE3-Cy3; green: NBD—G(RG)$_2$D-OH), 0.05 mgmL-1 Cy5-Glucose Oxidase (D) (magenta: Cy5-Glucose Oxidase; green: Sulforhodamine B) or 0.05 mgmL^{-1} Cy5-Urease (E) (magenta: Cy5-Urease; green: Sulforhodamine B) upon addition of 30 mM ACA. The scale bar of all the images is 5 μm, and all experiments were performed in triplicate (N = 3). For confocal microscopy images of the full cycle, see Figure S17–21.

Conflict of Interests

The authors declare no conflict of interest.

Data Availability Statement

The data that support the findings of this study are available from the corresponding author upon reasonable request.

[1] Y. Zhang, J. Y. Kang, M. Liu, Y. Huang, *RNA. Biol.* **2023**, *20*(1), 893–907.
[2] S. Boeynaems, S. Alberti, N. L. Fawzi, T. Mittag, M. Polymenidou, F. Rousseau, J. Schymkowitz, J. Shorter, B. Wolozin, L. Van Den Bosch, P. Tompa, M. Fuxreiter, *Trends. Cell. Biol.* **2018**, *28*(6), 420–435.
[3] P. B. Sehgal, J. Westley, K. M. Lerea, S. Di Senso-Browne, J. D. Etlinger, *Anal. Biochem.* **2020**, *597*, 113691.
[4] S. F. Banani, H. O. Lee, A. A. Hyman, M. K. Rosen, *Nat. Rev. Mol. Cell Biol.* **2017**, *18*(5), 285–298.
[5] A. A. Hyman, C. A. Weber, F. Jülicher, *Annu. Rev. Cell Dev. Biol.* **2014**, *30*, 39–58.
[6] C. P. Brangwynne, C. R. Eckmann, D. S. Courson, A. Rybarska, C. Hoege, J. Gharakhani, F. Jülicher, A. A. Hyman, *Science* **2009**, *324*, 1729–1732.
[7] W. T. Snead, A. S. Gladfelter, *Mol. Cell.* **2019**, *76*(2), 295–305.
[8] J. M. Lee, H. M. Hammaren, M. M. Savitski, S. H. Baek, *Nat. Commun.* **2023**, *14*(1), 201.
[9] M. R. Santoro, S. M. Bray, S. T. Warren, *Annu. Rev. Pathol.* **2012**, *7*, 219–45.
[10] C. D'Incal, J. Broos, T. Torfs, R. F. Kooy, W. Vanden Berghe, *Cells* **2022**, *11*(8), 1325.
[11] J. Boekhoven, A. M. Brizard, K. N. K. Kowlgi, G. J. M. Koper, R. Eelkema, J. V. Esch, *Angew. Chem.* **2010**, *122*, 4935–4938.
[12] L. S. Kariyawasam, C. S. Hartley, *J. Am. Chem. Soc.* **2017**, *139*, 11949.
[13] G. Ashkenasy, T. M. Hermans, S. Otto, A. F. Taylor, *Chem. Soc. Rev.* **2017**, *46*, 2543.
[14] P. Gobbo, A. J. Patil, M. Li, R. Harniman, W. H. Briscoe, S. Mann, *Nature Materials* **2018**, *17*, 1145–1153.

ChemSystemsChem

Research Article
doi.org/10.1002/syst.202400083

Chemistry Europe
European Chemical
Societies Publishing

[15] W. Liu, C. Lupfer, A. Samanta, A. Sarkar, A. Walther, *J. Am. Chem.Soc.* **2023**, *145*, 7090–7094; .

[16] M. G. Howlett, A. H. J. Engwerda, R. J. H. Scanes, S. P. Fletcher, *Nat. Chem.* **2022**, *14*, 805–810.

[17] T. M. Hermans, N. Singh, *Angew. Chem. Int. Ed.* **2023**, *62*, e202301529.

[18] S. Maiti, I. Fortunati, C. Ferrante, P. Scrimin, L. J. Prins, *Nature Chem.* **2016**, *8*, 725–731.

[19] Z. Zhang, M. G. Howlett, E. Silvester, P. Kukura, S. P. Fletcher, *J. Am. Chem. Soc.* **2024**, *146*(27), 18262–18269.

[20] A. Reja, S. Pal, K. Mahato, B. Saha, M. Delle Piane, G. M. Pavan, D Das, *J. Am. Chem. Soc.* **2023**, *145*(38), 21114–21121.

[21] S. Roy, J. Laha, A. Reja, D. Das, *J. Am. Chem. Soc.*.

[22] C. Donau, J. Boekhoven, *Trends in Chemistry* **2023**, *5*, 45–60.

[23] A. D. Slootbeek, M. H. I. van Haren, I. B. A. Smokers, E. Spruijt, *Chem. Commun.* **2022**, *58*, 11183–11200.

[24] D. Zwicker, R. Seyboldt, C. A. Weber, A. A. Hyman, F. Jülicher, *Nature Phy.* **2017**, *13*, 408–413.

[25] W. M. Aumiller, C. D. Keating, *Nat. Chem.* **2016**, *8*, 129.

[26] K. K. Nakashima, J. F. Baaij, E. Spruijt, *Soft Matter* **2018**, *14*, 361–367.

[27] C. Donau, F. Späth, M. Sosson, B. A. K. Kriebisch, F. Schnitter, M. Tena-Solsona, H.-S. Kang, E. Salibi, M. Sattler, H. Mutschler, J. Boekhoven, *Nat Commun* **2020**, *11*, 5167.

[28] F. Späth, C. Donau, A. M. Bergmann, M. Kränzlein, C. V. Synatschke, B. Rieger, J. Boekhoven, *J. Am. Chem. Soc.* **2021**, *143*(12), 4782–4789.

[29] C. Donau, F. Späth, M. Stasi, A. M. Bergmann, J. Boekhoven, *Angew. Chem. Int. Ed.* **2022**, *61*, e202211905.

[30] F. Späth, A. S. Maier, M. Stasi, A. M. Bergmann, K. Halama, M. Wenisch, B. Rieger, J. Boekhoven, *Angew. Chem. Int. Ed.* **2023**, *62*, e202309318.

[31] C. M. E. Kriebisch, L. Burger, O. Zozulia, M. Stasi, A. Floroni, D. Braun, U. Gerland, J. Boekhoven, *Nat. Chem.* **2024**, *16*, 1240-1249.

[32] S. M. Poprawa, M. Stasi, B. A. K. Kriebisch, M. Wenisch, J. Sastre, J. Boekhoven, *Nat Commun* **2024**, *15*, 4204.

[33] W. V. Leeuwen, C. Rabouille, *Traffic* **2019**, *20*, 623–638.

[34] N. Chen, Z. Zhao, Y. Wang, R. Dimova, *ACS Macro Lett.* **2020**, *9*, 1844–1852.

[35] D. Del Giudice, S. Di Stefano, *Acc. Chem. Res.* **2023**, *56*, 889–899.

[36] D. Del Giudice, F. Frateloreto, C. Sappino, S. Di Stefano, *Eur. J. Org. Chem.* **2022**, e202200407.

[37] E. Olivieri, A. Quintard, *ACS Org. Inorg. Au* **2023**, *3*, 4–12.

[38] Y. Qin, Y. Sung Sohn, X. Li, R. Nechushtai, J. Zhang, H. Tian, I. Willner, *Angew. Chem. Int. Ed.* e202415550.

[39] C. Biagini, F. Di Pietri, L. Mandolini, O. Lanzalunga, S. Di Stefano, *Chem. Eur. J.* **2018**, *24*, 10122–10127.

[40] C. Biagini, G. Capocasa, V. Cataldi, D. Del Giudice, L. Mandolini, S. Di Stefano, *Chem. Eur. J.* **2019**, *25*, 15205–15211.

[41] C. Biagini, G. Capocasa, D. Del Giudice, V. Cataldi, L. Mandolini, S. Di Stefano, *Org. Biomol. Chem.* **2020**, *18*, 3867–3873.

[42] D. Del Giudice, E. Spatola, M. Valentini, C. Bombelli, G. Ercolani, S. Di Stefano, *Chem. Sci.* **2021**, *12*, 7460–7466.

[43] D. Del Giudice, M. Valentini, G. Melchiorre, E. Spatola, S. Di Stefano, *Chem. Eur. J.* **2022**, *28*, e202200685.

[44] D. Del Giudice, E. Spatola, M. Valentini, G. Ercolani, S. Di Stefano, *ChemSystemsChem* **2022**, *4*, e202200039.

[45] D. Del Giudice, M. Valentini, C. Sappino, E. Spatola, A. Murru, G. Ercolani, S. Di Stefano, *J. Org. Chem.* **2023**, *88*, 4379–4386.

[46] M. Valentini, F. Frateloreto, M. Conti, R. Cacciapaglia, D. Del Giudice, S. Di Stefano, *Chem. Eur. J.* **2023**, *29*, e202301835.

[47] G. Capocasa, F. Frateloreto, S. C. Cavallari, M. Valentini, O. Lanzalunga, S. Di Stefano, *Chem. Eur. J.* **2024**, *30*, e202303897.

[48] M. Valentini, G. Ercolani, S. Di Stefano, *Chem. Eur. J.* **2024**, *30*, e202401104.

[49] A hollow structure is observed in all these cases, *i.e.*, pSS (both 75 and 150 kDa) and pSSM, with the exception of Dex, where the coacervates normally dissolve.

[50] I. B. A. Smokers, B. S. Visser, A. D. Slootbeek, W. T. S. Huck, E. Spruijt, *Acc. Chem. Res.* **2024**, *57*, 1885–1895.

[51] M. Kang, C. A. Day, A. K. Kenworthy, E. Di Benedetto, *Traffic* **2012**, *13*, 1589–1600.

[52] S. F. Vanier, G. Larouche, R. P. Wurz, A. B. Charette, *Org Lett.* **2010**, *12*, 672–675.

[53] H. Taylor, N. Gao, S. Mann, *Angew. Chem. Int. Ed.* **2023**, *62*, e202300932.